Journal of Organometallic Chemistry 880 (2019) 175–186

Contents lists available at ScienceDirect

Journal of Organometallic Chemistry

journal homepage: www.elsevier.com/locate/jorganchem

The photochemical and photophysical properties of the $[[M_3(dppm)_3(CO)]]^{2+}$ clusters (M = Pd, Pt)☆

Pierre D. Harvey

Département de chimie, Université de Sherbrooke, Sherbrooke, PQ, J1K 2R1, Canada

ARTICLE INFO

Article history:
Received 28 September 2018
Received in revised form
1 November 2018
Accepted 3 November 2018
Available online 7 November 2018

ABSTRACT

This title clusters were first reported by Puddephatt and his group over 30 years ago, and their reactivity was thoroughly investigated, namely including the oxidative additions of inorganic and organic substrates and host-guest associations. Then, Mugnier and Harvey, scrutinized in large detail the rich electrochemical behaviour of the $[[Pd_3(dppm)_3(CO)]]^{2+}$ cluster, $[Pd_3^{2+}]$, namely of the reduced paramagnetic species $[Pd_3^{\bullet+}]$ during the 1997–2010 period. Concurrently, Harvey and his group conducted an in depth study, starting about 2008 until now, of the rather equally rich photophysical properties of both $[M_3^{2+}]$ (M = Pd, Pt) clusters. This mini-review of 39 references focusses on these properties, which have never been reviewed before. Their excited state properties such as the presence of higher and lower energy triplet excited states, triplet-triplet energy transfers in assemblies and upconversion, as well as the strong electron acceptor behaviour of $[Pd_3^{2+}]$ are discussed. Impressive ultrafast rates of electron transfer (<85 fs) between electron donors such as porphyrin and tetrabenzoporphyrin derivatives and this cluster have been reported.

Contents

1. Introduction 175
2. Conclusion 183
Acknowledgments 185
Supplementary data 185
References 185

1. Introduction

Puddephatt reported the syntheses of the $[M_3(dppm)_3(CO)]^{2+}$ clusters ($[M_3^{2+}]$; M = Pd ($[Pd_3^{2+}]$), Pt ($[Pt_3^{2+}]$); dppm = bis(diphenylphosphino)methane; Fig. 1) in the mid-80s [1,2]. As dicationic species, these 42-electron clusters are accompanied by counter anions, generally $CF_3CO_2^-$ or PF_6^-. Rapidly, the host-guest chemistry of these species was readily revealed when halide anions were found to bind strongly on top of the unsaturated M_3 triangles with M … X^- separations indicating the presence of electrostatic contacts [2,3]. He then reviewed his work on the thermal chemistry of the title clusters in 1990 [4]. Subsequently, Braunstein also noted that $[Pd_3^{2+}]$ exhibits stronger binding affinity than the structurally related cluster $[PtPdCo(\mu\text{-dppm})_2(CO)_3(CN^tBu)]^+$ for example [5]. In this particular case, the PtPdCo center carries only a +1 charge leading to a lesser electrostatic strength with the halides. This information provided the first clue on the host-guest traits.

Mugnier and Harvey quickly realized there was an opportunity to exploit this strong binding behaviour for electrochemically driven C-X and Pd-X bond activations in organic and inorganic compounds, namely upon reducing $[Pd_3^{2+}]$ with one electron to form the highly reactive paramagnetic species $[Pd_3^{\bullet+}]$. Indeed, an in depth investigation was then undertaken, which was reviewed in 2004 [6]. This research continued several years after this publication [7–14]. Interestingly, the study of the electrochemical

☆ This article is dedicated to Prof. Richard J. Puddephatt (75th).

E-mail address: pierre.harvey@usherbrooke.ca.

https://doi.org/10.1016/j.jorganchem.2018.11.009
0022-328X/

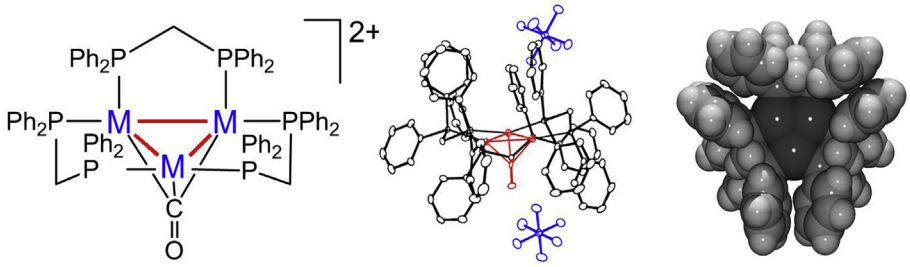

Fig. 1. Left: Drawing of the title clusters (M = Pd, Pt). Middle: example of an X-ray structure of a $[Pd_3(dppm)_3(CO)]^{2+}$ cluster as a PF_6^- salt. Right: space filling model showing the cavity above the M_3 center.

processes also led to the discovery of novel and innovating electrocatalytic reactions [6]. Concurrently, Harvey et al. figured out that the size of the hydrophobic cavity formed by the phenyl groups of the dppm bridging ligands above the naked M_3 face played a major role in the binding strength and selectivity [15], and this « picket fence basket » could accommodate larger substrates such as organic anions [16–19]. The model exhibiting an enlargement of the cavity was achieved by replacing the dppm ligand by dpam, bis(diphenylarsino)-methane, $[Pd_3(dpam)_3(CO)]^{2+}$. This concept turned out to be convenient as it mimics the enlargement of the cavity upon exciting $[M_3^{2+}]$ clusters as the M-M bond length increases in the triplet excited states (T_n and T_1; details provided below). A larger investigation of the ground state host guest properties of $[Pd_3^{2+}]$ indicated its clear affinity for organic substrates bearing arylcarboxylates [20]. This conclusion turned out to be crucial since it defined a suitable and simple access to the functionalization of these clusters via supramolecular assemblies. This mini-review presents the photophysical properties of the $[M_3^{2+}]$ clusters (M = Pd, Pt) including the presence of higher and lower energy triplet excited state behaviour, triplet-triplet energy transfer in assemblies and upconversion, as well as ultrafast rates of electron transfer when acting as acceptor for $[Pd_3^{2+}]$.

Earlier works. The spectroscopic analysis of the $[M_3^{2+}]$ clusters (M = Pd, Pt) was first reported in 1993 [21]. The nature of the lowest energy excited states was experimentally addressed using UV–visible, emission and polarized excitation spectroscopy, and emission lifetime measurements, and computationally (EHMO). The spectra at 77 K in glassy matrices are more resolved than those at 298 K and permit to observe more features. Indeed, the UV–visible spectra exhibit low-intensity shoulders at ~570 mm ($\varepsilon = 1500\ M^{-1}cm^{-1}$; $[Pd_3^{2+}]$) and at 460 nm ($\varepsilon = 3200\ M^{-1}cm^{-1}$; $[Pt_3^{2+}]$), which were assigned to $S_0 \rightarrow T_1$ absorptions ($^3A_2$, $^3E \leftarrow {}^1A_1$); essentially triplet $d\sigma \rightarrow d\sigma^*$. The representation of the $d\sigma^*$ orbital for example, symmetry a_2 in the C_3v point group, is provided in Fig. 2 (left).

The more intense bands located at 483 nm ($\varepsilon = 43400\ M^{-1}cm^{-1}$; $[Pd_3^{2+}]$) and 413 nm ($\varepsilon = 10900\ M^{-1}cm^{-1}$; $[Pt_3^{2+}]$) were assigned to the spin-allowed $^1E \leftarrow {}^1A_1$ ($a_2 \leftarrow e$) transition. $[Pd_3^{2+}]$ emits weakly at ~705 nm at 77 K (quantum yield, $\Phi_e < 0.001$; Fig. 2 right). It was then believed to be a T_1 emission but a subsequent study demonstrated that this emission came from an upper T_n state (see energy diagram in Fig. 3 right) [22].

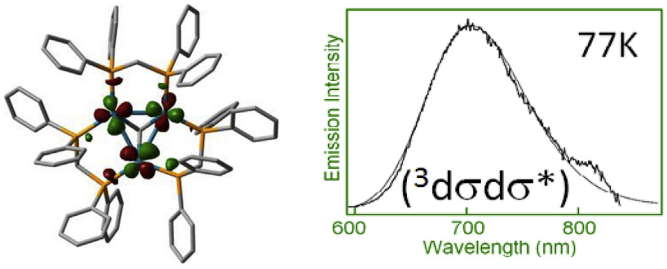

Fig. 2. Representation of the $d\sigma^*$ MO of $[Pd_3^{2+}]$ (left) and its triplet T_n state emission in 2-MeTHF at 77 K (right). The straight line is a simulated spectrum (detail below).

Concurrently, $[Pt_3^{2+}]$ is luminescent at 77 K ($\lambda_{max} = 650$ nm) with emission lifetimes, τ_e (77 K), of 14.0 ± 0.4 μs (PrCN), and 3.73 ± 0.05 μs (solid state), indicating the presence of a T_1 emission. The quantum yield, Φ_e (77 K) is ~0.013 in 2-MeTHF solution. No luminescence was detected at 298 K but the excited lifetimes measured from picosecond flash photolysis measurements, were respectively 80 ± 10 ps and 80 ± 10 ns for M = Pd and Pt, in 2-MeTHF. The shorter lifetime for $[Pd_3^{2+}]$ is clearly counter-intuitive at one would expect a heavy atom effect pushing the T_1 lifetimes of the Pt-species being shorter. The first clue in trying to explain this curious behaviour is the rather low intensity of the emission spectra (extremely low for $[Pd_3^{2+}]$) suggesting very efficient deactivation, thus corroborating the rather short ps time decay (80 ps at 298 K) from (transient absorption spectroscopy) TAS measurements. The second clue, is the rather very different absorption signature of the clusters (data mentioned above; $[Pt_3^{2+}]$ is yellow, and $[Pd_3^{2+}]$ is purple). The answer to this enigma came later when fs-laser technology became available (below).

The influence of guest molecules on the excited state properties of the title clusters was also investigated afterward [23]. By changing the solvent, the guest molecule inside the cavity is automatically different (*i.e.* a solvent molecule displacing the weakly bound $CF_3CO_2^-$ and PF_6^- counter anions). For $[Pt_3^{2+}]$ at 298 K, ps-TAS measurements indicated that $\tau(T_1)$ varies as 310 (MeOH), 300 (CD_3OD), 230 (C_6H_6), 190 (EtOH), 140 (MeOH saturated with $MeCO_2Na$), 80 (2-MeTHF), and 70 (Ph-Me) ns. Based on the fact that excited states are often deactivated by colliding with the solvent, the longer lifetimes suggest a lesser degree of solvent M_3^{2+} interactions. MeOH does not interact as $\tau(T_1)$ does not vary for CD_3OD. This observed variation indicates that PhMe and 2-MeTHF penetrates well the cavity, as well as acetate and benzene illustrating clearly the hydrophobic and dicationic nature of the cavity. At 77 K, the rigidity of the glasses slows down the collision effect, so the T_1 lifetime increases in the μs time scale (between 10.2 and 18.0 μs) with PhMe being again the solvent with the shortest value. This observation suggests that the Me group must preferentially penetrate that cavity and let anticipate a possible photo-induced C–H bond activation. For $[Pd_3^{2+}]$, these earlier ps-TAS measurements at 298 K indicated that $\tau(T_n)$ varies as 80 ps (THF), 39 ± 10 (PhMe), $<25 \pm 10$ (EtOH), and $<25 \pm 10$ ps (CH_3CN). Because the pulse width of the laser was 25 ps (so the limit of the time-resolution at that time), then the uncertainties prevent a reliable ordering of EtOH and CH_3CN (*i.e.* $\tau(T_n) < 25$ ps). Also note that $\tau(T_n) = 207$ ps when MeOH is the solvent (data from Ref. [22]), which is also the situation where the cavity is free from substrate.

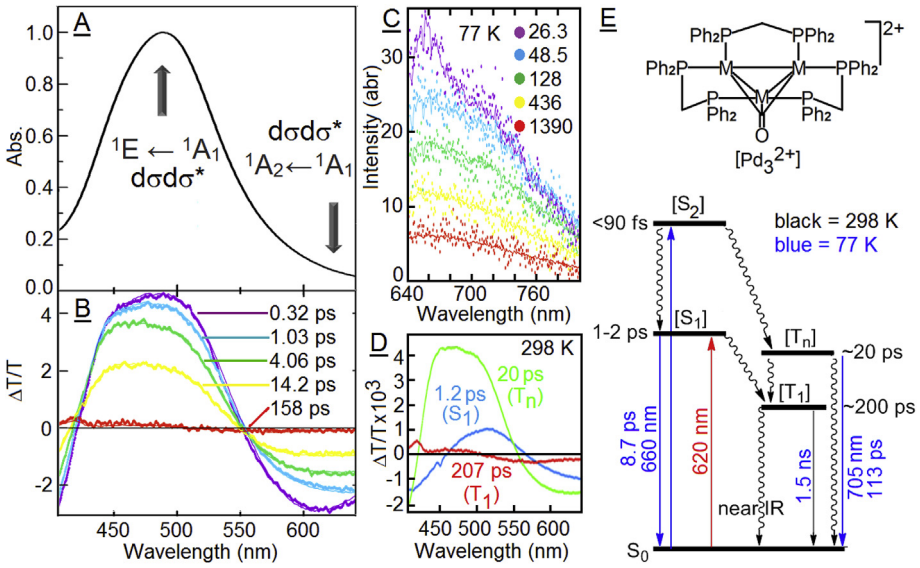

Fig. 3. A: absorption spectrum of $[Pd_3^{2+}]$ (as a PF_6^- salt) in CH_3OH at 298 K showing the positions of the two spin-allowed dσdσ* transitions (*i.e.* $^1A_2 \leftarrow {}^1A_1$ is forbidden by symmetry). B: time evolution of the fs-TAS signal of $[Pd_3^{2+}]$ in CH_3OH at 298 K. C: time-resolved fluorescence spectra of $[Pd_3^{2+}]$ in a 1:1 CH_3OH/2-MeTHF mixture at 77 K (delay times are in ps and the spectra are uncorrected due to the use of a Streak camera, whereas that shown in Fig. 2 is corrected). D: decay associated spectra of the fs-TAS measurements showing the three different species of $[Pd_3^{2+}]$ in CH_3OH at 298 K. E: state diagram of $[Pd_3^{2+}]$ showing the positions of the band maxima or shoulder in the various spectra (the lifetimes in black and in blue are for 298 and 77 K data, respectively) [22]. (For interpretation of the references to colour in this figure legend, the reader is referred to the Web version of this article.)

In this same article, the $\tau(T_n)$ value was reported to be $< 25 \pm 10$ ps for $[Pd_3^{2+}]$ in EtOH either saturated in Ar(g) or O_2(g), essentially meaning at the limit of the time resolution of the apparatus. This time scale also means that if any photo-induced reaction with O_2 occurs, for example the formation of $^1O_2$, it must occur with O_2 already sitting inside the cavity. Indeed, the excited state lifetime of this cluster (*i.e.* <25–35 ps) in solution is far too short to have O_2 diffusing efficiently towards the Pd_3^{2+} center for interactions (the time scale for the O_2 diffusion in organic solvents is ~2.5 ns). Therefore any photo-processes is unimolecular (*i.e.* pre-assembled). The $[Pd_3^{2+}]$ gets photo-oxidized in the presence of O_2 to form the 44-electon cluster $[Pd_3(dppm)_3(O_2)_2]^{2+}$ [24]. The final product was identified by FAB mass spectrometry and IR where the $\nu(O_2)$ modes were observed at 838 and 866 cm^{-1} (*i.e.* peroxide type). Interestingly, this cluster interacts with O_2 with a weak binding constant, K_{11}, of 730 M^{-1}. Because the quantum yield ($\Phi_{reaction}$) of 0.033 ± 0.004 (*i.e.* ~3%; measured by comparative actinometry with $[Fe(oxalate)_3]^{2+}$), the combination of the weak K_{11} with $\Phi_{reaction}$ strongly suggests that $[Pd_3^{2+}]$ in its dσ* ($^3A_2$) state efficiently transfers its energy to $^3O_2$ inside the pocket formed by the dppm ligands to transform it into the highly reactive $^1O_2$ just above the Pd_3^{2+} triangle, which in turn oxidizes the Pd_3^{2+} center ($^3[Pd_3^{2+}]^* \ldots {}^3O_2 \rightarrow [Pd_3^{2+}] + {}^1O_2$).

Similar to the ps-TAS study above describing the solvent effect on the triplet lifetime of $[Pd_3^{2+}]$, a recent fs-TAS investigation referring to the data presented in Fig. 3 (ref. [22]) also showed which of the three excited states of $[Pd_3^{2+}]$ is more prone to exhibit changes in lifetimes. A good example is the $PhCO_2^-$ (as a Na^+ salt) substrate (K_{11} ~10000 M^{-1} [21]) as illustrated in Table 1.

The S_1 and T_n state are not or weakly affected by the increasing number of equivalents of substrates *vs.* $[Pd_3^{2+}]$. Concurrently, $\tau(T_1)$ is more sensitive. Noteworthy, considering the datum for MeOH makes $\tau(T_n)$ varies as 207 (MeOH), 80 ps (THF), 35 ± 10 (PhMe), $<25 \pm 10$ (EtOH) and $<25 \pm 10$ ps (CH_3CN), suggesting the relative order of host-guest interactions in the T_1 excited state, with MeOH being the solvent generating an "empty" cavity. The conclusion is 2-fold. First, the capacity to detect an effect of a given substrate onto an excited state lifetime depends on the time scale of the lifetime (the longer, the more sensitive), meaning that deactivation proceeds by a collisional mechanism (like O_2). Second, because K_{11} is relatively small, the number of equivalents must be large in order to have a sufficient amount of assembled $PhCO_2^- \ldots [Pd_3^{2+}]$ species in solution. Table 1 presents essentially average values coming from the assembled and free $[Pd_3^{2+}]$ species. The effect of the number of equivalents on the photophysical parameters needs to be kept in mind below in the section describing the photo-induced electron transfers.

Both $[M_3^{2+}]$ clusters (Pd, Pt) undergo photoinduced oxidative degradation when in the presence of chlorocarbons ($[M_3^{2+}]^* + Cl\text{-}R \rightarrow M(dppm)Cl_2$; where R = CCl_3, $CHCl_2$, CH_2Cl, C_6H_5, $C_{10}H_{15}$ (adamantyl)) [25]. The K_{11} values turn out to be predictably extremely small ($0.2 < K_{11} < 36\ M^{-1}$) as these are neutral molecules, and unsurprisingly, $\Phi_{reaction}$ were found extremely weak as well ($0.00005 < \Phi_{reaction} < 0.003$; where adamantyl-Cl is the smallest). The tentative analysis of the data was rather complicated since the overall efficiency of the reaction depended simultaneously upon K_{11} (which depends upon the M_3^{2+} charge *vs.* the substrate polarity), the cavity-substrate hydrophobic interactions, the cavity size *vs.* substrate dimension; the C–Cl bond strength, and the reduction potential of the R–Cl substrate. Indeed, when the substrate was $PhCH_2$-Cl, the reaction proceeded thermally, a process that is aided by a rather weak C–Cl bond strength (69 kcal/mol). Moreover, using DFT computations, the optimized geometry of a model $[Pd_3(PH_3)_6(CO)]^{2+} \ldots C\text{–}CH_3$ assembly exhibited an average Pd···Cl separation of 2.83 Å, which is longer than that calculated for

Table 1
Excited lifetimes extracted from fs-TAS of $[Pd_3^{2+}]$ upon addition of $PhCO_2Na$ in MeOH [22]. Note that MeOH is the best solvent to have an empty cavity.

# eq.	$\tau(S_1)$ (±0.3 ps)	$\tau(T_n)$ (±0.5 ps)	$\tau(T_1)$ (±9 ps)
0	1.2	19.8	207
1	1.1	18.7	138
2	1.0	18.9	149
4	0.9	20.3	148
8	0.9	16.5	77

$[Pd_3(PH_3)_6(CO)]^{2+}$ … Cl^- (2.628 Å). This result illustrates the significant contribution of the electrostatic interactions in the latter assembly. Interestingly, the 2-electron electrochemical dissociative oxidation of $[Pd_3^{2+}]$ in the presence of R–Cl substrate also led to the same final Pd(dppm)Cl_2 product [26]. This astonishing resemblance with the photo-oxidative reactivity discussed above suggests that the $^3(d\sigma d\sigma)^*$ can also act as a reducing agent. This conclusion suggests that the photo-induced C–H bond activation with the $[M_3^{2+}]$ clusters (Pd, Pt) is also possible but its efficiency may be problematic.

The conclusion of these three last investigations together is that the title clusters in their $^3A_2$ ($d\sigma d\sigma^*$) state are capable of energy transfer and oxidative C-X bond activation all inside the pocket of the dppm ligands above the M_3^{2+} chromophore [23–25]. However, a question remains: how come a substrate as bulky as adamantyl-Cl undergoes a photo-induced C–Cl bond activation? The answer stems in the earlier DFT computations of the optimized geometries of the clusters. After optimizing the geometry of $[Pd_3^{2+}]$ and observing an excellent agreement with the X-ray data, the optimized geometries in the $^3A_2$ (d(Pd–Pd) = 2.778; d(Pd–P) = 2.376 Å) and ^3E (d(Pd–Pd) = 2.881, d(Pd–P) = 2.339 Å) states were obtained. Significant bond lengthening from its optimized geometry in the ground state $^1A_1$ is computed (d(Pd–Pd) = 2.592; d(Pd–P) = 2.317 Å; X-ray data, d(Pd–Pd) = 2.595 (17); d(Pd–P) = 2.311 (10) Å [25]), leading to an enlargement of the cavity with calculated P···P separations going from 3.257 to 3.901 Å. Thus, the pocket size increases upon irradiation and then let the large adamantyl substrate penetrate a little bit deeper inside the cavity somewhat enough to undergo C–Cl bon cleavage. This value of excited state distortion (ΔQ = 2.778–2.592) of 0.186 Å, was tested against a Franck-Condon analysis based on Heller's theory applied to electronic spectroscopy. It involves the use of wavefunctions which include both the electronic transition moment between two Born-Oppenheimer potential surfaces and the ground-state vibrational wavefunctions. The wavefunctions are then displaced in the wave packet and evolve with time according to the time-dependent Schrödinger equation, generally in the ps time scale. Both band maximum and fwhm are related to the relative "vibronic hot band" populations. For the Pd_3^{2+} frame, these Raman active modes the a_1 and e $\nu(Pd_2)$ modes (i.e. 204 and 143 cm^{-1}, respectively, see the Raman spectrum in Fig. 4). These two modes respectively give ΔQ = 0.172 and 0.199 Å, and a good match between the simulated spectrum and the experimental one (see the simulated spectrum in Fig. 2, right). The average value of these two are ΔQ ~0.186 Å, which is in complete agreement with that calculated by DFT above (also 0.186 Å). For $[Pt_3^{2+}]$ cluster, the average ΔQ ~ 0.33 Å ($\nu(Pt_2)$ = 149 (a_1), 125 (e) cm^{-1}). The discrepancy between the average ΔQs between the two clusters was unexplained but the new DFT computations using better basis sets [22] indicated that the M-M bond distances in the T_1 states were 2.832 ($[Pd_3^{2+}]$; which is similar as the previous calculations) and 2.867 Å ($[Pt_3^{2+}]$, which is smaller but more realistic).

Recent works. Over the past 10 years, the photochemistry of the title clusters focussed on $[M_3^{2+}]$ clusters within supramolecular assemblies with various mono-, bi- and tetracarboxy-derivatives of tetraarylporphyrin(metal) (M = Zn, Ni, FeCl), and with various derivatives of tetracarboxyphenyltetrabenzoporphyrinzinc(II). The main excited state behaviours are the S_1 and T_1 bi-directional energy and reductive electron transfers and upconversion.

Prior to describe the assemblies generated by the carboxy-derivatives and the $[M_3^{2+}]$ clusters, a discussion on the localization of the T_1 excited state of $[Pd_3^{2+}]$ is necessary. For about 24 years, it was believed that the weak triplet emission of this cluster located at about 705 nm stems from T_1 (Fig. 2, right [21]). Two problems persisted. First, the excited state lifetime measured by ps-TAS was in the >25–80 ps range. This time scale is unusually short for a transition metal complex. Usually a μs time scale is expected for T_1 emission. Indeed, the τ_e value for $[Pt_3^{2+}]$ is ~12–15 μs at 77 K. Second, the amount of material necessary to observe this 705 nm band was unusually large because it was weak. It is only recently that based on the calculated position (DFT) of the T_1 levels of the $[M_3^{2+}]$ clusters (1433 nm, M = Pd; 818 nm, M = Pt) using the difference in total energies of the optimized geometries of the clusters in their S_0 ($^1A_1$) and T_1 ($^3A_2$) levels, that a debate was triggered [22]. Experimentally, the position of the T_1 emission for the $[Pt_3^{2+}]$ cluster is 650 nm [22], which makes the calculated value (818 nm) over evaluated somewhat (*i.e.* ~3000 cm^{-1} too low). Because $[Pd_3^{2+}]$ reacts with $^3O_2$ in its triplet excited state *via* a primary energy transfer

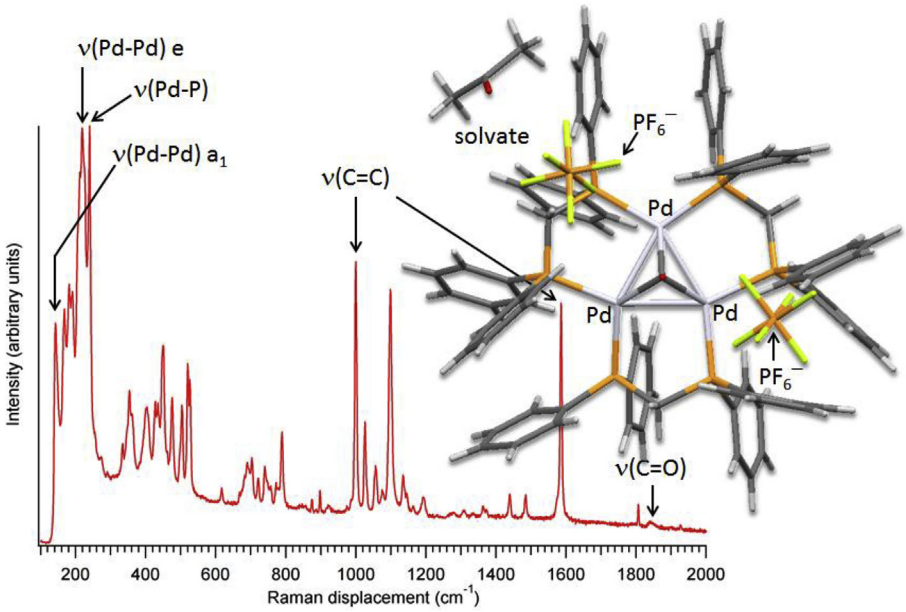

Fig. 4. FT-Raman spectrum and X-ray structure of $[Pd_3^{2+}]$ (as PF_6^- salt) [28].

process [24], then experimentally the position of the T_1 level of $[Pd_3^{2+}]$ is at least the same or higher than that of the $^1O_2$ ($^1\Delta_g$; ≤ 7882.4 cm^{-1}, ≥1269 nm)). This conclusion also makes the calculated 1433 nm value over evaluated (by ~900 cm^{-1}). The mystery was finally resolved when time-resolved spectroscopy (using a streak camera) detected two lifetimes for this 705 nm band at 77 K (113 ps and 1.5 ns) while using larger amount of materials. The larger value (1.5 ns) is reasonable for a T_1 lifetime when the excited state level is very low in energy (*i.e.* close to the S_0 level so that the non-radiative internal conversion processes are efficient). The former value (113 ps) is a time scale that resembles those observed at 298 K (<25–80 ps). The longer-lived species (1.5 ns) results from a triplet-triplet annihilation ($^3[Pd_3^{2+}]^*$ (T_1) + $^3[Pd_3^{2+}]^*$ (T_1) → $^3[Pd_3^{2+}]^*$ (T_n) + $[Pd_3^{2+}]$ (S_0) + heat) where the $^3[Pd_3^{2+}]^*$ (T_n) is issued from an upconversion process, and the 113 ps-species are issued from a simple 1-photon process. This mechanism was confirmed by using $[Pd_3^{2+}]$ (as PF_6^- salt) in the solid state (*i.e.* maximum concentration possible) and steady state laser excitation, where for the first time the observation of the 705 nm emission was made at 298 K (Fig. 5) [26].

For an upconversion to a state that emits at 705 nm (*i.e.* 14180 cm^{-1}), the two excited states interacting must have an energy of at least 7090 cm^{-1} (1410 nm). Because again $[Pd_3^{2+}]$ photogenerates $^1O_2$, then its T_1 energy is at least 7882.4 cm^{-1}, which is enough ($2 \times 7882.4 = 15765\ cm^{-1}$; 634 nm) for triplet-triplet annihilation and upconversion processes. Unfortunately, the T_1 emission in this cluster remained undetected in the 800–1400 nm range, which is consistent with its rather short lifetime (1.5 ns, instead of the expected μs time scale; therefore accompanied by a low emission quantum yield). Note that commercial near-IR detectors are also not particularly sensitive either.

Assemblies with the carboxy-tetraarylporphyrin derivatives and the $[M_3^{2+}]$ clusters. Evidence for assemblies can be provided by X-ray crystallography, ^{31}P NMR and UV–visible spectroscopy. Fig. 6 (left) exhibits two examples where the $CF_3CO_2^-$ substrate is placed inside the cavity of $[Pd_3^{2+}]$ [20] and a chiral $[Pd_3(dppm^*)_3(CO)]^{2+}$ version (dppm* = (*S,S*)-bis(bis(o-anisylphenylphosphino)methane) [27]. The two Pd···O contacts are 2.68 (5) and 2.75 (5) Å [20] and 2.572 (4) and 2.651 (4) Å [27], indicating that the interactions remain strongly electrostatic in nature.

Similarly, an example of the ^{31}P NMR and UV–visible monitoring of the binding of a carboxylate derivative onto $[Pd_3^{2+}]$ is presented in Fig. 6 (top right). The empty cavity exhibits a ^{31}P resonance in the vicinity of −3.12 ppm (bottom right), whereas the filled cavity (by a carboxylate derivative) shows a NMR peak at −8.17 ppm. Concurrently, upon adding a solution containing the monocarboxy(tetraphenyl)porphyrin(chloroiron(III)) into a solution of $[Pd_3^{2+}]$ in methanol, the UV–vis spectra exhibit an increase in the porphyrin signature (see upward arrows) and isosbestic points illustrating the 1:1 binding process (bottom middle). The binding constants, K_{11}, can be evaluated by performing one of the three different analyses (or average of all three) called Benisi-Hildebrand, Scatchard, and Scott plots [28]. The measurements are the most reliable when all three graphical methods give the same K_{11} value. For the title clusters, this was the case for all assemblies. A comparison of the K_{11} values for various carboxylate derivatives is provided in Fig. 7 issues from three thorough investigations [20,27,29]. As the $R-CO_2^-$ substrate becomes electron richer (by adding other $-CO_2^-$ substrates or replacing the chloroiron(III) by nickel(II), palladium(II) and zinc(II)), the K_{11} value increases illustrating again the electrostatic nature of the binding. The most striking evidence comes from the comparison of the K_{11} values of both title clusters with the same carboxylate derivative; K_{11} is almost identical regardless of the cluster ($[Pd_3^{2+}]$ or $[Pt_3^{2+}]$; Figs. 7 and 8) [30].

Quenching of the $^{1,3}[M_3^{2+}]^*$ clusters. The excited state behaviour of both title clusters in their triplet excited states were again first investigated a long time ago [23] where the excited state lifetimes were found somewhat dependent on the nature of the solvent inside the cavity. However, this type of behaviour only reflect on the nature of the solvate-cavity interactions, and non-radiative internal conversion processes may dictate the resulting lifetime ($\tau_e = 1/[k_P + k_{iP}]$; k_P is the radiative rate constant of the triplet state, and k_{iP} is the non-radiative rate constant from this same triplet state). In other words, no energy transfer occurs with the solvent molecules (obviously). Excited state quenching can occur in multiple manners. The most

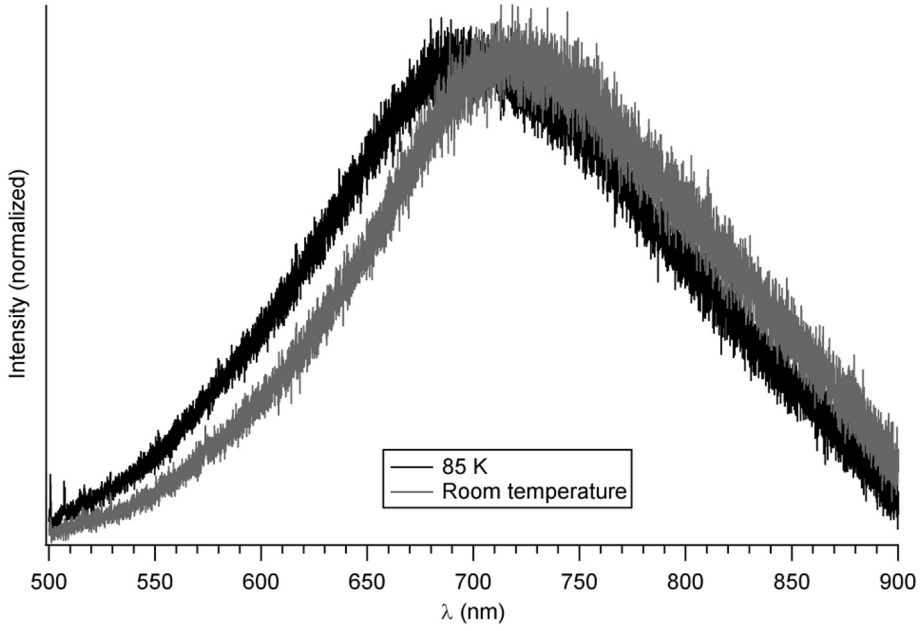

Fig. 5. Solid state emission of $[Pd_3^{2+}]$ (as PF_6^- salt) at 85 (black) and 298 K (grey) using laser excitation [26].

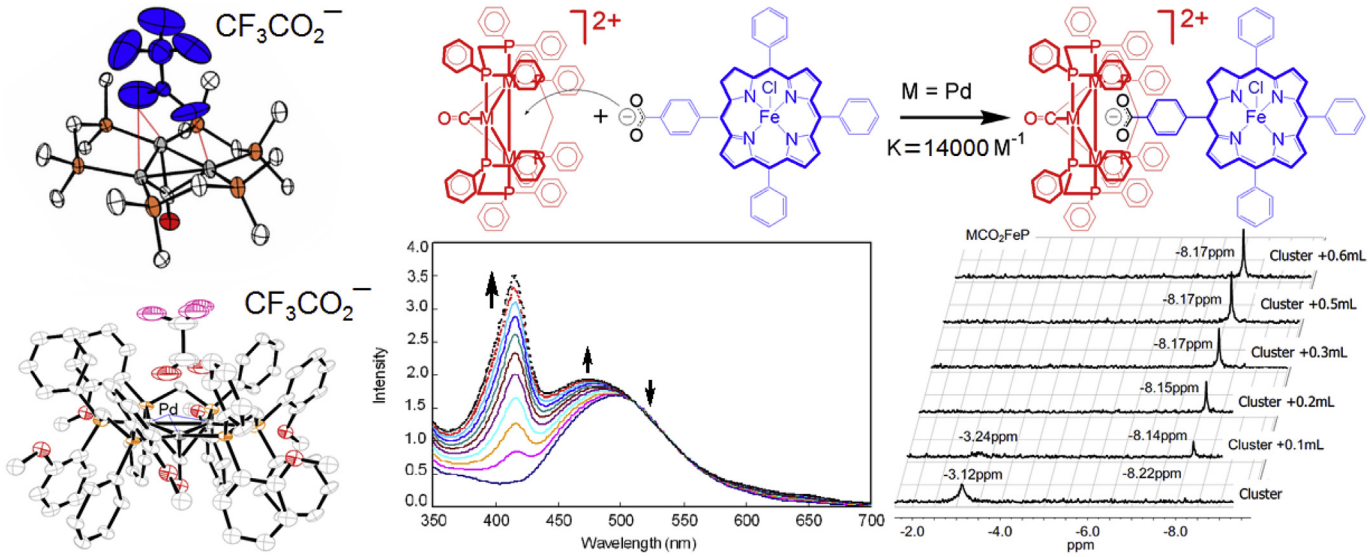

Fig. 6. Left: two examples of X-ray structures of carboxylate derivatives interacting with the Pd_3^{2+} center (achiral and chiral versions). Right: monitoring of the binding of the monocarboxy(tetraphenyl)porphyrin(chloroiron(III)) with [Pd_3^{2+}].

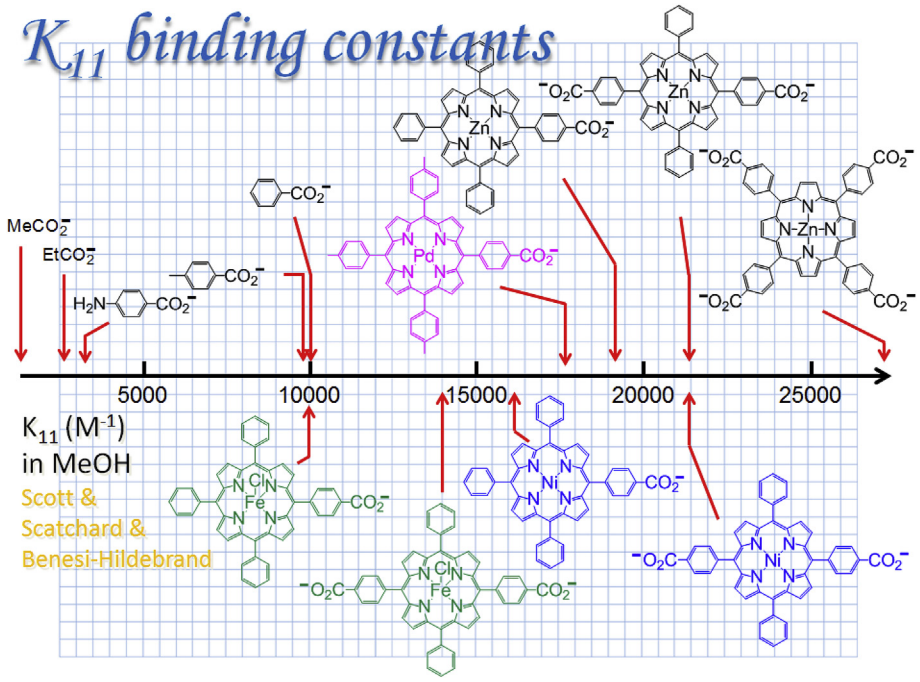

Fig. 7. Comparison of the average K_{11} values extracted from the Benisi-Hildebrand, Scatchard, and Scott plots (3) for the assemblies of [Pd_3^{2+}] with various carboxylate derivatives in methanol at 298 K by UV–vis spectroscopy. Note that K_{11} for O_2 is the same as for acetate (720 M^{-1}).

common processes are the energy and electron transfers. From the long standing electrochemical investigations, [Pd_3^{2+}] is notoriously known to be an electron sponge as it can have multiple reduced oxidation states (*i.e.* $[Pd_3]^n$ with n = +2, +1, 0, −1, and −2) [29]. Thus, for electron transfer processes for excited state quenching, the [Pd_3^{2+}] cluster can act as an electron acceptor. Indeed, the [Pd_3^{2+}] + 1 e^- → [$Pd_3^{\bullet+}$] process (PF_6^- salt) occurs at −0.50 V *vs.* SCE in THF containing 0.2 M of Bu_4NPF_6 (see peaks A_1 in Fig. 9 (left)) [31]. Using the cyclic voltammograms and the position of the 0-0 fluorescence and phosphorescence peaks of the derivatives of tetraphenylporphyrinzinc(II), [porphyrinzinc(II)], their excited state driving forces for photo-induced electron transfers ^{1}[porphyrinzinc(II)]* → [porphyrinzinc(II)]$^{\bullet+}$ + $1e^-$ and ^{3}[porphyrinzinc(II)]* → [porphyrinzinc(II)]$^{\bullet+}$ + $1e^-$ can be estimated (+1.0 ± 0.2 V and +0.7 ± 0.2 V *vs.* SCE). The conclusion is that the S_1 and T_1 state electron transfers to [Pd_3^{2+}] are thermodynamically favourable by respectively +0.5 and + 0.2 V. However, the smaller value for the triplet state (+0.2 V) may be not large enough to overcome the activation barrier associated with kinetic considerations (*i.e.* the rate could be very small). In conclusion, the ^{1,3}[Pd_3^{2+}]* species are prone to both energy and electron transfers.

The most striking evidence for an energy transfer process between [Pd_3^{2+}] and porphyrin derivatives is found in the complete quenching of the T_n emission at 705 nm (Fig. 4) when in the

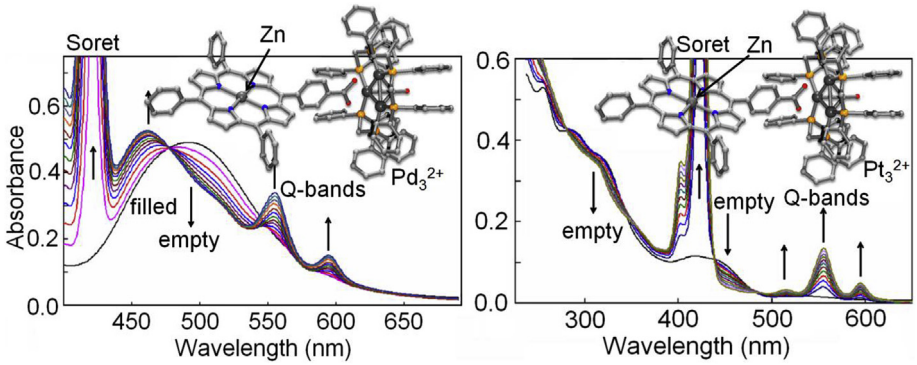

Fig. 8. Spectral evolution of the UV–vis spectra of $[M_3^{2+}]$ in methanol at constant concentration upon adding a solution containing mono-carboxy(tetraphenyl)porphyrin-zinc(II) (**MCP**) at 298 K [30].

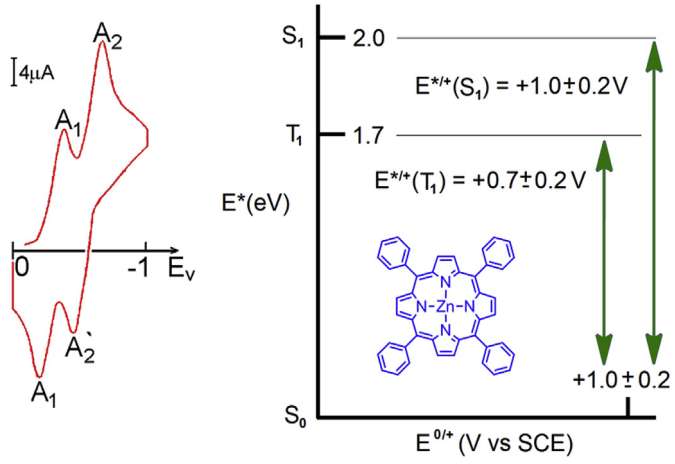

Fig. 9. Left: Cyclic voltammogram of $[Pd_3^{2+}]$ (as PF_6^- salt) in THF containing 0.2 M Bu_4NPF_6. Right: modified Latimer diagram of tetraphenylporphyrinzinc(II) species showing their 1st oxidation potential of ($E^{0/+}$) vs S_1 and T_1 state energies (E^*) giving rise to their corresponding estimated excited state driving forces, $E^{*/+}$, for electron transfer.

presence of mono- and di-carboxytetraphenylporphyrin(metal) with metal being chloroiron(III) [28]. Indeed, this larger oxidation state for M(III) precludes any efficient electron transfer in both directions ($[Pd_3^{2+}]$ is hard to oxidized; $E^{0/+} = +0.95$ V *vs.* SCE [13]). Moreover, the first spin-allowed d-d level is placed in the vicinity of 775 nm (12900 cm^{-1}) based on data reported for μ-oxobis[tetraphenylporphyriniron(III)] (*i.e.* 3 unpaired electrons) [32]. So energy transfer from the T_n level of $[Pd_3^{2+}]$ (705 nm) to the d-d level of the mono- and di-carboxytetraphenylporphyrin(chloroiron(III)) (~775 nm) is possible. The complete quenching of the 705 nm emission indicates that efficient energy transfer occurring at a time scale that is shorter than 113 ps. The rate of transfer was not measured in this work but this conclusion is consistent with the later study on the rate of through space energy transfer in a octaethylposphyrin-ethane-octaethyl … porphyrin-nickel(II) dyad [33]. Indeed in this case, the time scale of transfer from the free base unit to the d-d level of the Ni(II) species is < 10 ps (which is obviously faster than 113 ps).

Interestingly, this duality in quenching mechanisms led to a marked acceleration of the rate of fluorescence quenching of tetraphenylporphyrinzinc(II) going from mono-, to di- to tetracarboxylate derivatives [34]. In all cases, the S_1 level (~630 nm; 15900 cm^{-1}) is placed above the T_n energy level of $[Pd_3^{2+}]$ (705 nm; 14200 cm^{-1}). So as the number of $[Pd_3^{2+}]$ bonded to the carboxylate groups increased from 1 to 2 to 4, the number of energy acceptors increased, and so the probability of transfers increased as well (by virtue of an increase of spectral overlap in a Forster Resonance Energy Transfer). Concurrently, this increase in number of $[Pd_3^{2+}]$ around the central tetraphenylporphyrinzinc(II) also increased the heavy atom effect, also resulting in a potential decrease in both singlet and triplet emission lifetimes. Finally, as the number of (negatively charged) carboxylate groups increased, the central tetraphenylporphyrinzinc(II) unit becomes more electron rich (as the K_{11} values demonstrate; Fig. 7), and thus more prone for photo-induced electron transfers. These three photophysical features all push in the same direction, resulting in an "exponential" effect on the quenching of the emissions of the central unit. A distinction between the various contributions appeared necessary and a series of thorough investigations followed [22,30,34–38].

Another earlier work reported an investigation on the energy transfer between the title clusters and mono-carboxytetraarylporphyrinmetal(II) [30]. Indeed, the $^3[Pt_3^{2+}]^*$ lifetime decreased slightly upon the formation of an assembly indicating slow quenching (Table 2). In parallel, the monitoring of the fluorescence (τ_F) and phosphorescence (τ_P) lifetimes and quantum yields (Φ_F, Φ_P) of ^{1,3}[porphyrin(metal)]* at both 298 and 77 K indicated that these parameters weakly affected by the presence of $[Pt_3^{2+}]$ meaning that no quenching takes place. This result is consistent with the fact that the T_1 level of $^3[Pt_3^{2+}]^*$ (here $\lambda_{max} = 650$ nm, but the spectrum starts at 600 nm; ~16700 cm^{-1}, energy donor) is placed above both S_1 and T_1 levels of the acceptor ^{1,3}[porphyrin(metal)]* (again ~630 nm; 15900 cm^{-1}). Concurrently during the course of the electrochemical studies on $[Pd_3^{2+}]$, $[Pt_3^{2+}]$ was also examined but the reduction potential was found much more negative (*i.e.* harder to reduce), explaining why no study was reported. This property also indicates that quenching by a photo-induced electron transfer from ^{1,3}[metalloporphyrin]* to $[Pt_3^{2+}]$ is

Table 2
Structure of the $[Pt_3^{2+}]$ … porphyrin assemblies, and comparison of the triplet emission lifetime (τ_e) of $[Pt_3^{2+}]$ at 77 K in the absence and the presence of substrate ($PhCO_2Na$ and mono-carboxytetraarylporphyrin(metal(II))).

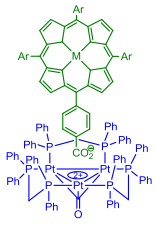

Substrate		τ_e (μs)	k_{ET} (s^{-1})
-		12.63 ± 0.07	-
$PhCO_2Na$		12.40 ± 0.05	no transfer
M	Ar		
Zn	Ph	9.57 ± 0.04	2.4×10^4
Zn	Tol	10.30 ± 0.03	2.1×10^4
Pd	Tol	11.80 ± 0.08	0.6×10^4

unfavourable. A change of the Ph groups for tolyls was also performed in order to increase the electronic density on [porphyrin(metal)], with the hope to promote photo-induced electron transfer. However, this modification did not change the quenching rate, k_Q, thus indicating absence of an electron transfer mechanism, and also corroborating that $[Pt_3^{2+}]$ is hard to reduce.

However, the situation is different for the $[Pd_3^{2+}]$ … porphyrin assemblies where a change in τ_F and τ_P of the mono-carboxytetraarylporphyrin(zinc(II)) was noted. The change in τ_F was 7 orders of magnitude larger at 298 over that at 77 K, which is fully consistent with the fact that rate of electron transfers decreases when the barrier of activation associated with the large reorganisation energy upon freezing the medium, increases. Concurrently, the rate of quenching, here k_{ET}, of the ^{3}[porphyrin(metal)]* species by $^3[Pd_3^{2+}]^*$ (T_1) in the assemblies for M = Pd and Ar = tolyl at 298 K is 0.7×10^4 s^{-1}. This rate is considered slow but not unusual for triplet-triplet energy transfer (see some examples in Table 3). Again a recent work focussed on increasing the electronic density at the porphyrin center by increasing the number of carboxylate groups in a way to that the triplet state of the porphyrin unit becomes more electron rich and more prone to photo-induced electron transfer to the electron acceptor $[Pd_3^{2+}]$ (Table 3) [34]. Using ns-TAS, the triplet lifetimes, τ_T, of the porphyrin chromophores were monitored and the rates of quenching, k_Q, were evaluated (note that $k_Q = k_{ET} + k_{et}$; et = electron transfer). For *MCO_2ZnP*, the quenching is dominated by energy transfer, but for *DCO_2ZnP* and *TCO_2ZnP*, electron transfer takes over. It is also reasonable to believe that k_{ET} increases with the number of $[Pd_3^{2+}]$ clusters surrounding the tetraarylporphyrinzinc(II) unit ([porphyrinzinc(II)]) but in a linear fashion.

For the S_1 state, fs-TAS was used to extract accurate k_{et} values for the reaction: ^{1}[porphyrinzinc(II)]* … $[Pd_3^{2+}]$ → [porphyrinzinc(II)]$^{\bullet+}$ … $[Pd_3^{\bullet+}]$, where [porphyrinzinc(II)] is *MCO_2ZnP* and *DCO_2ZnP* [35]. Because the sensitivity of the analyses depends on the binding constants K_{1x} (x = 1, 2 or 4), which in turn dictate the relative amount of the various possible assemblies present in solution for a given number of relative equivalents (as Table 1 indicates that the resulting lifetimes are an average of all species in solution), it becomes important to know the amount of each assemblies and try to maximize the assembled species (see examples in Table 4 [35]). However, it is important not to use large excesses of $[Pd_3^{2+}]$ to avoid of cluttering the fs-TAS spectra with many species at the same time. A typical example is given in Fig. 10. By performing the measurements of the fs-TAS instrument for various ratios (*i.e.* 1:1, 1:2, 1:4; Table 4), it is possible to monitor the various signals that grows (*i.e.* charge separated state) and to make the appropriate assignment. For the provided example, the species with relaxation lifetimes of » 8 ns, 65.5 ps, and 1.91 ns are respectively the triplet T_1, non-emissive S_1 ··· solvent assembly through the zinc metal, and fluorescent S_1 species of **MCP**, of the free dye. It represents 44.2% of the total amount (*i.e.* free dye not associated with $[Pd_3^{2+}]$). The red-shifted signal at 427 nm is the typical signature of the radical cation [porphyrinzinc(II)]$^{\bullet+}$ (55.8%), here tetraphenylporphyrinzinc(II). However, this cation is readily formed within the laser pulse (FWHM = 85 fs in these measurements) meaning that the $k_{et} > 1.2 \times 10^{13}$ s^{-1} (*i.e.* 1/(<85 fs)). This rate is ultrafast.

In order to demonstrate that the large electronic density drives the process, in addition to the **TCP** dye, three other "enriched" [porphyrinzinc(II)]-containing dyes were designed and investigated (Fig. 11) [36,37]. The binding constants, K_{1x}, increase expectedly with the number of conjugations and the planarity of the π-systems. The energy change, ΔE, for the reaction ^{1}[porphyrinzinc(II)]* … $[Pd_3^{2+}]$ → [porphyrinzinc(II)]$^{\bullet+}$ … $[Pd_3^{\bullet+}]$ is evaluated from the driving force, $E^{*/+}$, for ^{1}[porphyrinzinc(II)]* → [porphyrinzinc(II)]$^{\bullet+}$ + $1e^-$, and the 1-e^- reduction potential of $[Pd_3^{2+}]$ ($[Pd_3^{2+}] + 1\ e^- \rightarrow [Pd_3^{\bullet+}]$; $E_{red} = -0.5$ V *vs.* SCE). The $E^{*/+}$'s are calculated from the S_1 energy (2.07 (**TCP**), 1.87 (**TCPBP**), 1.68 (**TCPEP**), 1.78 (**TCPEBP**) eV) minus the 1-e^- oxydation potential ([porphyrinzinc(II)] → [porphyrinzinc(II)]$^{\bullet+}$ + $1e^-$; E_{ox} = +0.81 (**TCP**), +0.76 (**TCPBP**), +0.70 (**TCPEP**), +0.46 (**TCPEBP**) V *vs.* SCE). The resulting ΔE's are all positive (thermodynamically favourable).

Similarly to **MCP** and **DCP**, the assemblies made with $[Pd_3^{2+}]$ and upon **TCP**, **TCPBP**, **TCPEP**, and **TCPEBP** also exhibit $k_{et} > 1.2 \times 10^{13}$ s^{-1} (*i.e.* 1/(<85 fs)). This observation supports the photoinduced electron transfer process as the quenching mechanism, all being ultrafast. Moreover, the resulting [porphyrinzinc(II)]$^{\bullet+}$ … $[Pd_3^{\bullet+}]$ charge separated species is not prone for a second electron transfer despite the fact there are other $[Pd_3^{2+}]$ units around the central [porphyrinzinc(II)] unit (Fig. 12 left). The only redox process possible is the back electron transfer (see Fig. 10, right, purple arrow). In all cases, the time scale for this process is short ps, which can also be considered ultrafast. The efficiency of this process (forward (fs) and back electron transfer (ps)) can also be viewed by an electron channeling through the π-system of the dye and through the contact between the π-MOs of the CO_2^- group and the LUMO of $[Pd_3^{2+}]$ (Fig. 12, right). Indeed, the various optimized geometries indicated the presence of a quasi-C_s symmetry in all cases (see one example in Fig. 12, center).

The last work concerned the electron richer **TCP**, **TCPBP**, **TCPEP**, and **TCPEBP** dyes [38] in comparison with the *MCO_2ZnP*, *DCO_2ZnP* and *TCO_2ZnP* in their T_1 state [34]. The primary conclusion was that as the electron density is increased, then the excited dyes become more reducing. The question is as the T_1 energy of these dyes decreases, will an electron transfer still take place? The data are placed in Table 5. The key issue is that the ΔE values for ^{3}[porphyrinzinc(II)]* … $[Pd_3^{2+}]$ → [porphyrinzinc(II)]$^{\bullet+}$ … $[Pd_3^{\bullet+}]$ are smaller (+0.13 < ΔE < +0.27 V *vs.* SCE, T_1) with respect to (+0.58 < ΔE < +0.76 V; S_1). The consequence is that k_{et} is slower (~50–150 ps time scale for T_1 compared to < 85 fs for S_1). Nonetheless, the corresponding rates (k_{et}) are also ultrafast. Concurrently, the back electron transfer, also called charge recombination (CR; with rates k_{CR}), takes place in the ns time scale, which is also slower than that observed for the S_1 level (short ps).

The conclusion is that despite the loss of energy upon relaxing from the S_1 to the T_1 levels of [porphyrinzinc(II)] dyes, the photo-induced electron transfer is still ultrafast. The reason stems from the rather low reduction potential of $[Pd_3^{2+}]$ (*i.e.* −0.5 V *vs.* SCE [6–14]). The other interesting feature is the long-lived charge separated state of the [porphyrinzinc(II)]$^{\bullet+}$ … $[Pd_3^{\bullet+}]$ species (>3 ns; see Table 5, 5th column), with a trend **TCP** < **TCPBP** < **TCPEP** < **TCPEBP**. Indeed because of this longer time scale, dyad dissociation may occur and the highly reactive species may escape the solvent cage (note that the time-scale for diffusion in common organic solvent is 2–3 ns). Knowing that the $[Pd_3^{\bullet+}]$ species is stable enough at the time scale of the cyclic voltammogram, and enough to record its electron paramagnetic resonance (EPR) spectrum [6], photocatalytic processes can be

Table 3
Comparison of the k_Q values of the quenching of the T_1 state of the porphyrin unit in the $[Pd_3^{2+}]$ … mono-, di- and tetra-carboxytetraarylporphyrinzinc(II) assemblies.

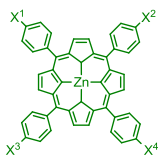

Code	*MCO_2ZnP*	*DCO_2ZnP*	*TCO_2ZnP*
X^1	Me	Me	CO_2^-
X^2	Me	CO_2^-	CO_2^-
X^3	Me	CO_2^-	CO_2^-
X^4	CO_2^-	Me	CO_2^-
k_Q (s^{-1})	2.1×10^4	1.1×10^5	5.6×10^7

Table 4
Relative percentages of the various assemblies of $[Pd_3^{2+}]$ *vs.* the mono- (**MCP**), di- (**DCP**) and tetra-carboxytetraarylporphyrin(zinc(II)) (**TCP**) species in a 4:1 ratio [35].[a]

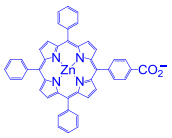

$K_{11} = 19300\ M^{-1}$ (%)

Por-$[Pd_3^{2+}]$	55.8

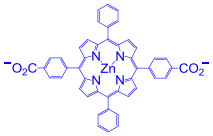

$K_{12} = 21700\ M^{-1}$ (%)

Por-$[Pd_3^{2+}]_2$	72.0
NaO_2C-Por-$[Pd_3^{2+}]$	21.3

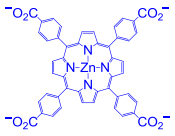

$K_{14} = 27500\ M^{-1}$ (%)

Por-$[Pd_3^{2+}]_4$	87.2
NaO_2C-Por-$[Pd_3^{2+}]_3$	11.2
$(NaO_2C)_2$-Por-$[Pd_3^{2+}]_2$	1.40
$(NaO_2C)_3$-Por-$[Pd_3^{2+}]$	0.18

[a] The remainder of the % is the unassembled porphyrin. Por = [porphyrinzinc(II)].

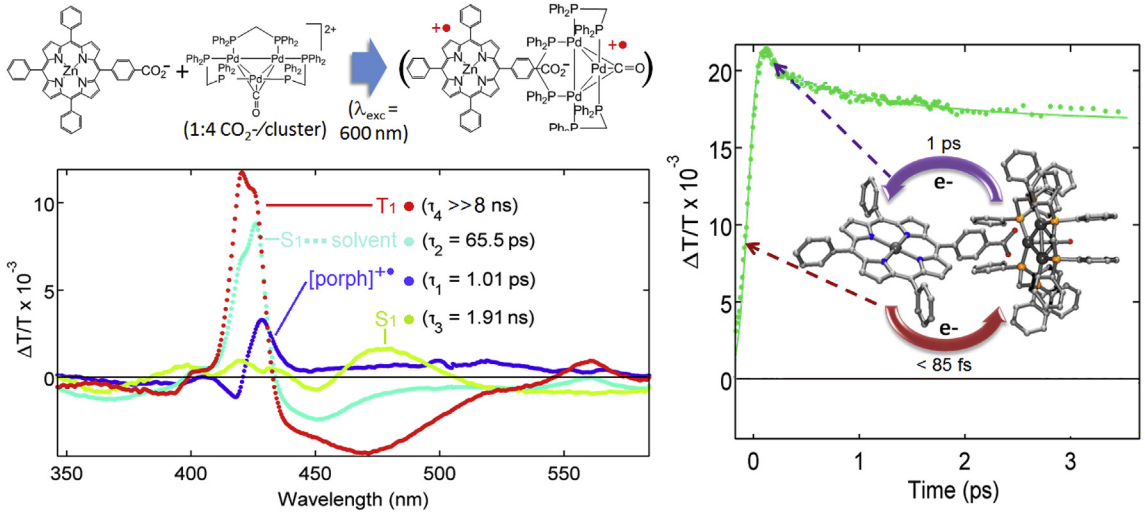

Fig. 10. Left: Decay associated spectra of the various species generated when **MCP** is mixed with $[Pd_3^{2+}]$ in CH_3OH in a 1:4 ratio ($\lambda_{exc} = 600$ nm; *i.e.* at the Q-bands). Values in parentheses are the excited state lifetimes of these species. Right: Time evolution of the signal at 427 nm (where the $[porphyrinzinc(II)]^{\bullet+}$ signal is higher). Laser FWHM = 85 fs.

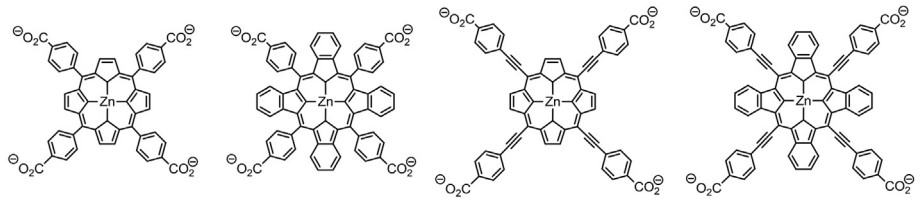

	TCP	TCPBP	TCPEP	TCPEBP
K_{1x} =	27500	38600	70400	83200 M^{-1}
ΔE =	+0.76	+0.61	+0.58	+0.72 V

Fig. 11. Structures of four porphyrin-containing dyes exhibiting extended π-system rendering them better electron donors. Below are the binding constants, K_{1x}, showing the increase in electronic density and the corresponding ΔE for the reaction occurring at the S_1 level: $^1[porphyrinzinc(II)]^*$ … $[Pd_3^{2+}] \rightarrow [porphyrinzinc(II)]^{\bullet+}$ … $[Pd_3^{\bullet+}]$.

sought, in replacement of the electrocatalytic ones. The two advantages would then be the absence of the often inconvenient supporting electrolyte in solution (needed to perform electrocatalytic reactions), and the convenient use of both the visible and near-IR light (*i.e.* solar irradiation). Indeed, the dye (here [tetrabenzoporphyrinzinc(II)]) acts as a strongly absorbing antenna and an electron donor at the same time, which is usually not a sacrificial redox agent.

Combined with the earlier studies on the triplet energy transfer $^3[porphyrinmetal]^* + [Pd_3^{2+}] \rightarrow [porphyrinmetal] + {}^3[Pd_3^{2+}]^*$ [22,35], the other main conclusion for this work, referring to Fig. 13, when X = H, CH_3, the triplet quenching occurs by energy transfer, but when X = CO_2^-, the quenching occurs by electron transfer.

2. Conclusion

Again, the title clusters were first reported by Puddephatt and his group, who explored in detail their rich thermal chemistry. Afterward, the equally rich electrochemical properties were studied by the Mugnier and Harvey groups in collaboration. Here, this mini-review demonstrated that the $[M_3^{2+}]$ species also exhibit rich photochemical and -physical traits. Despite the significant amount

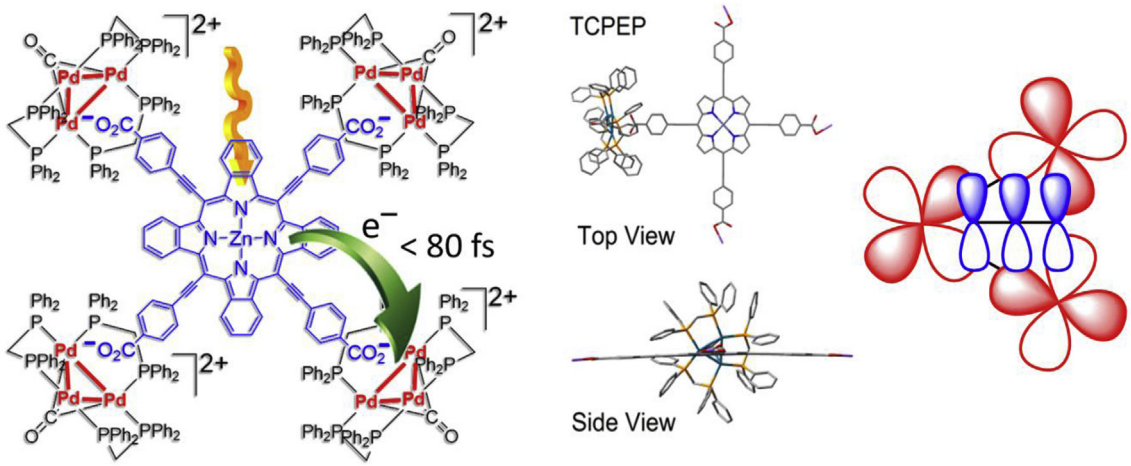

Fig. 12. Left: Illustration of a photo-induced electron transfer from [porphyrinzinc(II)] (here **TCPEBP**) to one of the $[Pd_3^{2+}]$ electron acceptors within a saturated assembly. Only one electron transfer can occur as the oxidized [porphyrinzinc(II)]$^{\bullet+}$ species is not reducing enough for a second transfer. Also note that the time-resolution of the apparatus was 80 fs in this specific experiment. Center: example of an optimized geometry (DFT) of a dyad composed of **TCPEP** and one $[Pd_3^{2+}]$ (plus three Na^+ atoms). Right: Illustration of the frontier MO contacts between the CO_2^- π-system (blue) and the LUMO of $[Pd_3^{2+}]$. Note that the computed LUMO of the $[M_3^{2+}]$ clusters is shown in Fig. 2 (left). (For interpretation of the references to colour in this figure legend, the reader is referred to the Web version of this article.)

Table 5
ps-ns transient absorption data for the ^{3}dyes* (dye = [porphyrinzinc(II)]).

dye	τ(^{3}dye* ··· $[Pd_3^{2+}]$ → dye$^{+\bullet}$ ··· $[Pd_3^{+\bullet}]$)	k_{et}, s^{-1} ($k = 1/\tau$)	ΔE V *vs* SCE	τ(dye$^{+\bullet}$ ··· $[Pd_3^{+\bullet}]$ → dye ··· $[Pd_3^{2+}]$)	k_{CR}, s^{-1} ($k = 1/\tau$)
TCPP	47.4 ps	2.11×10^{10}	+0.27	3.3 ns	30×10^7
TCPBP	105 ps	0.95×10^{10}	+0.23	(15.9 ns)[b]	~6.3×10^7[b]
TCPEP	157 ps	0.64×10^{10}	+0.13	(89 ns)[b]	~1.1×10^7[b]
TCPEBP	100 ps	1.00×10^{10}	+0.27	(146 ns)[b]	~0.7×10^7[b]

[a] Significant decomposition prevents the accurate estimation of the lifetime and energy transfer rate.
[b] The delay line is 8 ns; the measured values become increasingly inaccurate as it exceeds this limit. The trend can be considered real. Note that $\tau(T_1)$ of the ^{3}dyes* without $[Pd_3^{2+}]$ is » 8 ns.

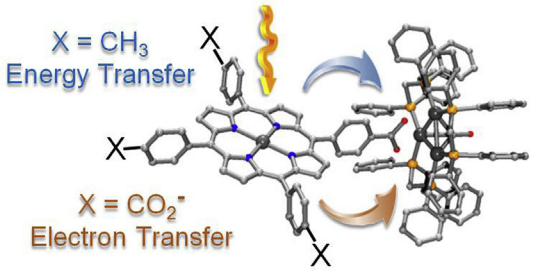

Fig. 13. Illustration of the quenching of ^{3}[porphyrinmetal]* … $[Pd_3^{2+}]$ based on X.

of reported investigations described herein, there are still relevant aspects that still need to be explored. In relation with the photo-induced C-X bond activation (X = Cl) [25], C–H bond activation was left unexplored. Indeed, ps-TAS measurements suggested that toluene, which is prone to C–H bond activation (E(C–H) = 377 kJ/mol), promotes significant $^3[M_3^{2+}]^*$ … solvent interactions (deduced from the comparison of $\tau(T_1)$ and $\tau(T_n)$ data in MeOH (empty cavity) *vs.* in toluene [23]). The primary products would the highly reactive corresponding hydrides "$[M_3(\mu_3\text{-}H)^{2+}]$", which is prone to chemically evolve. For the $[Pd_3(\mu^3\text{-}H)^{n+}]$ species (n = 1, 2), this product would be stable at least at the time scale of the cyclic voltammetry as previously demonstrated [8]. However, characterization of palladium hydride species by X-ray crystallography is also found extremely rare in the literature, and to the best of our knowledge only one work related to the $[Pd_3^{2+}]$ species concerns the X-ray characterization of the $[Pd_4(dppm)_4(H)]^+$ cluster [39]. Concurrently, the corresponding $[Pt_3(\mu^3\text{-}H)^{n+}]$ species (notably n = 1) should be more stable as demonstrated by Puddephatt [5]. It now appears relevant to investigate the photochemistry of $[Pt_3^{2+}]$, because of the intuitively more stable corresponding photoproducts, but also for the significantly longer excited state lifetimes in solution at 298 K (*i.e.* ns time scale). The photo-induced electron transfer reactivity of $[Pt_3^{2+}]$ has not been investigated in detail in the earlier investigation [30], but now it appears evident that the amount of assembled dyads [porphyrinzinc(II)] … $[Pt_3^{2+}]$ in 1:1 ratio and a K_{1x} value of ~20000 M^{-1} was not appropriate in these cases as it generates only 20% of assemblies. This situation combined with a more negative reduction potential of $[Pt_3^{2+}]$ compared to $[Pd_3^{2+}]$ (unpublished), leading to more modest changes in emission lifetimes of the dyes in the [porphyrinzinc(II)] … $[Pt_3^{2+}]$ dyads (since the k_{et} values will be smaller), then the detection of any photo-induced electron transfer would prove difficult. A revisit with larger ratios appears pertinent.

Finally, based on all past works on the $[M_3^{2+}]$ clusters, this skeleton appear particularly robust and the characterization of the photoproducts should be facile. For examples, oxidative additions of terminal η^2-ethynyl-containing aromatics to both $[Pd_3^{2+}]$ [18] and $[Pt_3^{2+}]$ [4] have been reported, where the C-M bonds are shown to be strong (*i.e.* K_{11} unmeasurably large). So far, the aromatics were simple phenyl derivatives. This strong bond offers an opportunity to avoid the problem related with the amplitude of the binding constant being an issue in the measurements. Moreover, the electronic communication across the M – C bond would be more pronounced. This feature means that depending on the nature of the R

functional group in the $[M_3(\eta^2\text{-}C{\equiv}CR)^+]$ skeleton (say for an example ferrocenyl/ferrocenium), would automatically alter their photophysical and -chemical properties significantly. Thus, the exploitation of the photochemical behaviour of these robust clusters appears unfinished, but the basis presented herein is obviously available.

Acknowledgments

PDH would like to acknowledge « Dick » (Puddephatt) for inspiration and positive encouragements in its own way while following the evolution of this research program from a distance over the years. He also would like to express his deepest thanks to Prof. Yves Mugnier, Université de Bourgogne, who became a dear friend, while working on the electrochemical behaviour of the palladium cluster. The author would also like to thank all the co-workers listed in the references for their important contributions to this topic. Throughout the years, the work was supported by the Natural Sciences and Engineering Research Council of Canada, and the Fonds de Recherche du Québec - Nature et Technologies.

Appendix A. Supplementary data

Supplementary data to this article can be found online at https://doi.org/10.1016/j.jorganchem.2018.11.009.

References

[1] L. Manojlović-Muir, K.W. Muir, B.R. Lloyd, R.J. Puddephatt, Synthesis and structure of a cluster complex containing the dication $[Pd_3(\mu_3\text{-}CO)(\mu\text{-}Ph_2PCH_2PPh_2)_3]^{2+}$, J. Chem. Soc. Chem. Commun. 0 (1983) 1336–1337, https://doi.org/10.1039/C39830001336.

[2] B.R. Lloyd, A. Bradford, R.J. Puddephatt, Coordinatively unsaturated clusters: the rapid reversible addition of two carbonyl ligands to a trinuclear platinum cluster, Organometallics 6 (1987) 424–427, https://doi.org/10.1021/om00145a032.

[3] B.R. Lloyd, R.J. Puddephatt, The mechanism of formation of the cluster $[Pd_3(\mu_3\text{-}CO)(\mu\text{-}Ph_2PCH_2PPh_2)_3]^{2+}$, Inorg. Chim. Acta. 90 (1984) https://doi.org/10.1016/S0020-1693(00)80736-7. L77–L78.

[4] R.J. Puddephatt, L. Manojlovic-Muir, K.W. Muir, Coordinatively unsaturated tripalladium and triplatinum clusters: models for reactions on metal surfaces, Polyhedron 9 (1990) 2767–2802, https://doi.org/10.1016/S0277-5387(00)84182-0.

[5] P.D. Harvey, K. Hierso, P. Braunstein, X. Morise, Comparison in halide binding ability between the unsaturated clusters $[Pd_3(\mu\text{-dppm})_3(CO)]^{2+}$ and $[PdPtCo(\mu\text{-dppm})_2(CO)_3(CN\text{-}t\text{-}Bu)]^+$ (dppm=$Ph_2PCH_2PPh_2$), Inorg. Chim. Acta. 250 (1996) 337–343, https://doi.org/10.1016/S0020-1693(96)05247-4.

[6] P.D. Harvey, Y. Mugnier, D. Lucas, D. Evrard, F. Lemaître, A. Vallat, Optical, electrochemical, and catalytic properties of the unsaturated host [Pd3(dppm)3(CO)]$^{2+}$and $Pd_4(dppm)_4(H)_2^{2+}$clusters: an overview, J. Cluster Sci. 15 (2004) 63–90, https://doi.org/10.1023/B:JOCL.0000027543.60768.3e.

[7] C. Cugnet, D. Brevet, S. Dal Molin, D. Lucas, Y. Mugnier, P.D. Harvey, Deoxygenation of nitrosobenzene by the electrogenerated $Pd_3(dppm)_3(\mu_3\text{-}CO)$ cluster, J. Cluster Sci. 18 (2007) 671–683, https://doi.org/10.1007/s10876-007-0135-8.

[8] C. Cugnet, D. Lucas, E. Collange, B. Hanquet, A. Vallat, Y. Mugnier, A. Soldera, P.D. Harvey, Generation, characterization, and electrochemical behavior of the palladium–hydride cluster $[Pd_3(dppm)_3(\mu_3\text{-}CO)(\mu_3\text{-}H)]^+$ (dppm=Bis(diphenylphosphinomethane), Chem. Eur J. 13 (2007) 5338–5346, https://doi.org/10.1002/chem.200700069.

[9] C. Cugnet, Y. Mugnier, S. Dal Molin, D. Brevet, D. Lucas, P.D. Harvey, Thermal and electrochemically assisted Pd–Cl bond cleavage in the d^9–d^9 $Pd_2(dppm)_2Cl_2$ complex by [Pd3(dppm)3(CO)]$^{n+}$ clusters (n = 2, 1, 0), Inorg. Chem. 46 (2007) 3083–3088, https://doi.org/10.1021/ic061777h.

[10] C. Cugnet, D. Lucas, F. Lemaître, E. Collange, A. Soldera, Y. Mugnier, P.D. Harvey, Unexpected reaction of the unsaturated cluster host and catalyst $[Pd_3(\mu_3\text{-}CO)(dppm)_3]^{2+}$with the hydroxide ion: spectroscopic and kinetic evidence of an inner-sphere mechanism, Chem. Eur J. 12 (2006) 8386–8395, https://doi.org/10.1002/chem.200600395.

[11] C. Salomon, S. Dal Molin, D. Fortin, Y. Mugnier, R.T. Boeré, S. Jugé, P.D. Harvey, The first unpaired electron placed inside a C_3-symmetry P-chirogenic cluster, Dalton Trans. 39 (2010) 10068–10075, https://doi.org/10.1039/c0dt00542h.

[12] D. Brevet, D. Lucas, P. Richard, A. Vallat, Y. Mugnier, P.D. Harvey, Formation and X-ray structure of the host–guest adduct $[[Pd3(dppm)3(CO)](NO_3)]^+$ and the mechanism of its electrochemical reduction, Can. J. Chem. 84 (2006) 243–250, https://doi.org/10.1139/v05-249.

[13] D. Brevet, D. Lucas, Y. Mugnier, P. Harvey, Electrochemical dissociative oxidation of the unsaturated [Pd3(dppm)3(CO)]$^{2+}$cluster; an astonishing resemblance with the photo-oxidative analogue, J. Cluster Sci. 17 (2006) 5–12, https://doi.org/10.1007/s10876-005-0013-1.

[14] D. Lucas, F. Lemaître, B. Gallego-Gómez, C. Cugnet, P. Richard, Y. Mugnier, P.D. Harvey, New insights into the stoichiometric and catalytic reactivity of unsaturated $Pd_3(dppm)_3CO^{n+}$clusters (n = 0, 1) towards halocarbons - first evidence for inorganic by-products, Eur. J. Inorg. Chem. 2005 (2005) 1011–1018, https://doi.org/10.1002/ejic.200400594.

[15] T. Zhang, M. Drouin, P.D. Harvey, The tuning of binding properties via the change in cavity size of unsaturated palladium trinuclear clusters, Chem. Commun. 0 (1996) 877–878, https://doi.org/10.1039/cc9960000877.

[16] S. Fournier, C. Cugnet, A. Vallat, C.H. Devillers, Y. Rousselin, M.M. Kubicki, D. Lucas, Y. Mugnier, P.D. Harvey, Reactivity of [Pd3(dppm)3(CO)] n+ and [Pd3(dppm)3(CO)](RCCR)$^{n+}$ (n = 0, +1, +2) towards F–. Evidence of Reactive Intermediates and X-Ray Structure of $[Pd_3(dppm)_3(MeO_2CC{\equiv}CCO_2Me)(F)]PF_6$, J. Cluster Sci. 21 (2010) 837–856, https://doi.org/10.1007/s10876-010-0338-2.

[17] C. Cugnet, S.D. Molin, D. Brevet, D. Lucas, Y. Mugnier, P.D. Harvey, R.T. Boeré, Alkyne adducts of paramagnetic and diamagnetic tripalladium clusters supported by dppm ligands, Can. J. Chem. 109 (2009) 103–109, https://doi.org/10.1139/V08-105.

[18] S. Dal Molin, C. Cugnet, D. Brevet, D. Lucas, Y. Mugnier, D. Fortin, R.T. Boeré, P.D. Harvey, Enhanced stability of a paramagnetic palladium complex promoted by interactions with ethynyl substrates, Organometallics 26 (2007) 5209–5215, https://doi.org/10.1021/om700377a.

[19] M. Rashidi, G. Schoettel, J.J. Vittal, R.J. Puddephatt, Triply bridging alkyne complexes of palladium, Organometallics 11 (1992) 2224–2228, https://doi.org/10.1021/om00042a042.

[20] R. Provencher, K.T. Aye, M. Drouin, J. Gagnon, N. Boudreault, P.D. Harvey, M. Drouin, Ground-state guest-host chemistry in the hydrophobic cavity of the unsaturated cyclic $Pd_3(dppm)_3CO^{2+}$Cluster, Inorg. Chem. 33 (1994) 3689–3699, https://doi.org/10.1021/ic00095a012.

[21] P.D. Harvey, R. Provencher, Lowest energy excited states of unsaturated cyclic $M_3(dppm)_3CO^{2+}$ clusters (M = Pd, Pt), Inorg. Chem. 32 (1993) 61–65, https://doi.org/10.1021/ic00053a010.

[22] P. Luo, P.L. Karsenti, B. Marsan, P.D. Harvey, Triplet energy transfers in well-defined host-guest porphyrin-carboxylate/cluster assemblies, Inorg. Chem. 55 (2016) 4410–4420, https://doi.org/10.1021/acs.inorgchem.6b00185.

[23] P.D. Harvey, S.M. Hubig, T. Ziegler, Spectroscopic and photophysical investigations of the unsaturated cyclic trinuclear clusters $M_3(dppm)_3CO^{2+}$(M = Pd, Pt). Evidence for excited-state guest-host chemistry, Inorg. Chem. 33 (1994) 3700–3710, https://doi.org/10.1021/ic00095a013.

[24] P.D. Harvey, M. Crozet, K.T. Aye, Photoinduced addition of dioxygen molecules in the unsaturated sites of the $Pd_3(dppm)_3CO^{2+}$ catalyst, Can. J. Chem. 73 (1995) 123–130, https://doi.org/10.1139/v95-019.

[25] P.D. Harvey, R. Provencher, J. Gagnon, T. Zhang, K. Hierso, M. Drouin, S.M. Socol, Photoinduced oxidative degradation of the $M_3(dppm)_3CO^{2+}$clusters (M = Pd, Pt) by chlorocarbons and chloride ion, Can. J. Chem. 02 (1996) 2268–2278, https://doi.org/10.1139/v96-255.

[26] B. Du, A. Langlois, D. Fortin, C. Stern, P.D. Harvey, Complete quenching of the $[Pd3(dppm)3(CO)]^{2+}$Cluster emission via electrostatic host-guest assemblies with carboxylate-containing tetraphenylporphyrins of Ni(II) and Fe(III), J. Cluster Sci. 23 (2012) 737–751, https://doi.org/10.1007/s10876-012-0470-2.

[27] C. Salomon, D. Fortin, C. Darcel, S. Jugé, P.D. Harvey, The first c3-symmetric P-stereogenic diphosphinomethane trinuclear palladium clusters: synthesis and characterization, J. Cluster Sci. 20 (2009) 267–280, https://doi.org/10.1007/s10876-009-0244-7.

[28] K.A. Connors, Binding Constants: the Measurement of Molecular Complex Stability, Wiley, 1987, https://doi.org/10.1016/0223-5234(87)90280-7.

[29] S.D. Molin, Y. Mugnier, D. Fortin, P.D. Harvey, The [Pd3(dppm)3(CO)]^n clusters (n = 1-,2-); Rare cases of anionic palladium species, Dalton Trans. 39 (2010) 8976–8981, https://doi.org/10.1039/c0dt00616e.

[30] S.M. Aly, C. Ayed, C. Stern, R. Guilard, A.S. Abd-El-Aziz, P.D. Harvey, Triplet energy transfers in electrostatic host-guest assemblies of unsaturated organometallic cluster cations and carboxylate-containing porphyrin pigments, Inorg. Chem. 47 (2008) 9930–9940, https://doi.org/10.1021/ic801006g.

[31] I. Gauthron, Y. Mugnier, K. Hierso, P.D. Harvey, Electrochemical reduction of the unsaturated cyclic trinuclear $Pd_3(dppm)_3CO^{2+}$ cluster, Can. J. Chem. 75 (1997) 1182–1187, https://doi.org/10.1017/CBO9781107415324.004.

[32] A.C. Banciu, On the electronic spectra and electronic structure of some square-pyramidal Fe(III) porphyrin complexes, Rev. Roum. Chem. 47 (2003) 805–811.

[33] V.S. Chirvonyi, V.A. Galievskii, A.M. Shulga, R. Gadonas, V. Krasauskas, A. Pyalakauskas, Picosecond kinetics of exchange of electron-excitation energy in mixed ethane-bisporphyrins containing Ni (II) and Cu (II) ions, Khim. Fiz. 12 (1993) 1073–1080.

[34] B. Du, C. Stern, P.D. Harvey, Singlet and triplet energy transfer rate acceleration by additions of clusters in supramolecular pigment-organometallic cluster assemblies, Chem. Commun. 47 (2011) 6072–6074, https://doi.org/10.1039/c1cc11174d.

[35] P. Luo, P.-L. Karsenti, G. Brisard, B. Marsan, P.D. Harvey, Are the orientation and bond strength of the $RCO_2^-\cdots M$ link key factors for ultrafast electron transfers? Chem. Commun. 51 (2015) 17305–17308, https://doi.org/10.1039/

C5CC06779K.
[36] P. Luo, P.-L. Karsenti, G. Brisard, B. Marsan, P.D. Harvey, Electron-transfer kinetics within supramolecular assemblies of donor tetrapyrrolytic dyes and an acceptor palladium cluster, Inorg. Chem. 55 (2016) 1894–1904, https://doi.org/10.1021/acs.inorgchem.5b02788.
[37] P. Luo, P.-L. Karsenti, G. Brisard, B. Marsan, P.D. Harvey, Ultrafast electron transfers in organometallic supramolecular assemblies built with a NIR-fluorescent tetrabenzoporphyrine dye and the unsaturated cluster $[Pd_3(dppm)_3(CO)]^{2+}$, Organometallics 35 (2016) 816–826, https://doi.org/10.1021/acs.organomet.6b00050.
[38] P. Luo, P.-L. Karsenti, B. Marsan, P.D. Harvey, Triplet energy *vs.* electron transfers in porphyrin- and tetrabenzoporphyrin-carboxylates/$[Pd_3(dppm)_3(CO)]^{2+}$ cluster assemblies; a question of negative charge, New J. Chem. 42 (2018) 8160–8168, https://doi.org/10.1039/C7NJ03943C.
[39] D. Evrard, D. Meilleur, M. Drouin, Y. Mugnier, P.D. Harvey, Characterization of a new tetranuclear cluster of palladium, $[Pd_4(dppm)_4(H)]^-$, Z. Anorg. Allg. Chem. 628 (2002) 2286–2292, https://doi.org/10.1002/1521-3749(200211)628, 11<2286::AID-ZAAC2286>3.0.CO;2-O.